IEEE Access
Multidisciplinary | Rapid Review | Open Access Journal

Received May 20, 2022, accepted June 6, 2022, date of publication June 13, 2022, date of current version June 16, 2022.

Digital Object Identifier 10.1109/ACCESS.2022.3182367

Shifting Process Optimization of Dedicated Hybrid Transmission

WEI REN[1], JUHUA HUANG[1], HUIHUI XU[2], JINJU YIN[2], CHONG LIU[2], AND LEI ZHANG[2]

[1]School of Mechatronics Engineering, Nanchang University, Nanchang, Jiangxi 330031, China
[2]Magna PT Powertrain (Jiangxi) Company Ltd., Nanchang, Jiangxi 330031, China

Corresponding author: Juhua Huang (huangjuhua6@163.com)

This work was supported by the Key Research and Development Program funded by Jiangxi Province under Grant 20192BBEL50014.

ABSTRACT The shifting process of a hybrid electric vehicle (HEV) could be implemented by a motor to simplify the control requirement when the clutch is engaged. In order to reduce the vehicle jerk and simplify the clutch control requirement during the shifting process, this paper introduces a 3-speed dedicated hybrid transmission (3DHT) with P1/P3 configuration and a power shift control strategy. A finite-time linear quadratic regulator (LQR) is proposed to smoothly transfer torque and suppress driveline oscillations during the torque transfer process with a maximum jerk of 5.6 m/s^3. Since the clutch stays engaged, a predictive sliding mode control (SMC) is proposed to track the speed of the sleeve quickly and precisely during the synchronization process, which takes 0.18s and maintains a speed difference of around 1 rpm. Furthermore, a Kalman Filter is utilized to overcome the difficulties associated with side shaft torque measurement and low wheel speed resolution. A simulation is performed in MATLAB/SIMULINK, and the powershift (2nd -> 3rd) is compared with other methods. The comparison indicates that the proposed power shift strategy can reduce the maximum jerk from 14.8 m/s^3 to 5.6 m/s^3, while the entire shifting process lasts for 0.71s. Therefore, the proposed power shift control strategy effectively improves the shift quality.

INDEX TERMS Hybrid electric vehicle, power shift, dedicated hybrid transmission, linear quadratic regulator, sliding mode control.

I. INTRODUCTION

In response to governmental regulations requiring energy savings and reduction of emissions, an increasing number of automobile manufacturers have reduced the production of traditional combustion engine vehicles and increased the production of all-electric vehicles [1], [2]. However, they are limited by the high costs of research and development, inadequate battery life, and the lack of charging facilities [3]–[5]. OEMs prefer hybrid vehicles to transition from combustion engine vehicles to all-electric vehicles [6]–[8]. The transmission of a hybrid vehicle integrates a motor, an inverter, and a control unit based on a traditional transmission. Per the location of the motor in the transmission system, a hybrid transmission is divided into 5 categories: P0, P1, P2, P3, and P4 [9], [10]. The hybrid transmission studied in this paper is a 3DHT with a P1/P3 structure. A motor-generator (MG1) is installed along with an engine via a pair of gears positioned before a clutch and is primarily used for series charging and for starting the engine. Another motor-generator (MG2) is connected to the ring gear of the final drive at the output shaft and is used for low-speed all-electric and parallel driving, and energy recovery and torque compensation during gear shifting.

Since the 3DHT incorporates a clutch and an MG1, it can shift like a conventional automatic manual transmission (AMT) or a clutchless automatic manual transmission (CLAMT). The clutch should disengage and engage the driveline in a traditional shifting process, which takes approximately 0.5s. Also, since the clutch is nonlinear, its actuation system should be accurately controlled to achieve the desired clutch torque [11]. However, during the shifting process of a CLAMT, speed synchronization of the clutch gear and the sleeve is performed by a motor without the actuation of the clutch. Therefore, the shifting process in a 3DHT can be similarly completed by the MG1 and the clutch stays engaged without actuation throughout the shifting process. This process can simplify the clutch control requirement and improve the clutch's service life. Various studies have been performed on speed synchronization during the shifting

The associate editor coordinating the review of this manuscript and approving it for publication was Ton Duc Do.

process without a clutch. Mo *et al.* [12] introduced an innovative bilateral Harpoon-shift synchronizer for a CLAMT, and Tseng *et al.* [13] proposed an advanced shifting control of synchronizer mechanisms for a CLAMT. Both of these studies employed a proportional-integral (PI) controller for regulating the clutch gear and sleeve speed. However, the PI controller achieves a slower speed synchronization and lower tracking accuracy than the SMC. Yu *et al.* [14] proposed an SMC for speed synchronization in a CLAMT during the shifting process, suppressing external disturbances and ensuring rapid convergence of the synchronization speed error. Fu *et al.* [15], [16] proposed a double SMC control scheme for a motor in an electric bus, which resulted in faster torque responses and reduced the steady-state error of speed control during the shifting process. Zhu *et al.* [17] proposed a robust optimal speed synchronization control scheme for a CLAMT based on LQR, which regulated speed synchronization precisely when subjected to a perturbation. Zhong *et al.* [18] introduced a coordinated control strategy based on feed-forward, bang-bang, and PID control for the speed synchronization of the engine in a CLAMT.

Another feature of the 3DHT is the integration of an MG2 with the final drive ring gear, which allows the 3DHT to shift without torque interruption. During the power shift process, the driving torque is transferred between the engine and MG2. The control of torque release and restoration is very important, since poor torque control may cause oscillations in the driveline system. Liang *et al.* [19], [20] introduced a novel clutchless power shift transmission system with a shifting control strategy and a power-sharing control strategy, which enabled power shift without torque interruption and greatly improved driving comfort. Li *et al.* [21] proposed an optimal control system for the power shift process of a dual-clutch transmission. A finite-time LQR was introduced for the optimal control of a clutch, which lowered the jerk during the shifting process. Nguyen *et al.* [22] studied the shifting strategy and energy management of a two-motor drive powertrain for extended-range electric buses. Modified bump functions were recommended to profile motor torque during the shifting process. However, the method for torque transfer only involved feedforward control, and robustness could not be guaranteed. Yang *et al.* [23] devised three alternative empirical polynomials to control torque reduction and reinstatement during the shifting process in an electric vehicle. However, the torque control in this case was also feedforward control, hence robustness could not be guaranteed. Teufelberger *et al.* [24] introduced an optimized control strategy of a DHT based on the calculation of quasi-stationary hybrid modes for torque and powertrain configuration. Zhao *et al.* [25] proposed a coordinated control strategy of a DHT based on a dynamic programming (DP) algorithm, which could shorten the shifting time and improve the shift quality. But it would lead additional slipping work on the clutch. Tao *et al.* [26] introduced a hybrid control strategy of a DHT which could optimize the fuel consumption and improve the drivability.

During the torque transfer phase in the driveline system, oscillations can be suppressed actively to improve vehicle drivability. Some studies have proposed active damping control strategies to improve drivability. Walker *et al.* [27] proposed an approach for actively suppressing transient responses in a motor via a PID controller, which successfully suppressed oscillations in a hybrid powertrain. Templin *et al.* [28] proposed an anti-jerk LQR controller for a traditional vehicle, which asymptotically followed the driver's demand torque to suppress driveline oscillations. However, the engine's response time was very long, while its torque control accuracy was low, and could not be easily implemented in an actual vehicle. Fredriksson [29] proposed an active damping LQR controller in a mild hybrid vehicle to damp out oscillations during vehicle acceleration. Syed *et al.* [30] proposed an active-damping-capable transaxle controller with a feedforward active compensator in an HEV, which significantly improved drivability by suppressing driveline resonance.

Energy management plays an essential role in an HEV and affects the vehicle's drivability and fuel economy. Model predictive control (MPC) has been widely utilized for energy management of HEV [22], [31], [32]. In [31], a DP algorithm was employed to solve the optimal solution problem based on pre-defined complete drive cycle information. In [32], a continuation/generalized minimal residual algorithm was proposed to obtain an optimal solution for engine power, MG power, and battery power. The temperature and state of charge (SOC) affect the battery discharge and charge power. Besides, the property of the MG is influenced by the temperature and the SOC of the battery. Therefore, the energy management of an HEV can influence the behavior of the shift quality. However, in this paper the energy management is not the main work, so the following assumptions are made during the shifting process: 1) the SOC of the battery is around 50%; 2) the temperature of battery is around 40°; 3) the MG can work in the maximum power for 5s.

This paper introduces a 3DHT system, including one engine and two motor-generators. Since the DHT has an MG1 before the clutch, there are two possible ways to achieve powershift. The first way is to shift based on the clutch actuation [21], [24], [25]. Due to the clutch's nonlinearity and hysteresis, it needs additional control requirements [11]. The second way is to shift with the clutch staying engaged like a shifting process of a CLAMT [12]–[14] which could simplify the control requirement of the clutch in the 3DHT. However, the driving modes of the studied 3DHT are much more complicated than a CLAMT. Coordinated torque control of the engine and MG2 should be established in the 3DHT to achieve a power shift. Besides, an active synchronization process is necessary when the clutch is engaged during the shifting process. The engine and MG1 are coupled with the input shaft due to the engaged clutch. It will increase the inertia at the clutch gear, and a significant speed difference can result in large frictional work between sleeve and clutch gear during mechanical synchronization. In [12], [13], the

speed synchronization relied on a PI controller. It had a longer duration and a higher static error than a conventional SMC [14]. A predictive SMC can obtain an optimal solution to balance the shift duration and the static error during an active synchronization process. The jerk should be considered to achieve a good shift quality in the shifting process. In [22], [23], a feedforward torque control was applied to reduce the jerk, which could not guarantee robustness. In [25], a low jerk was achieved through a forward discrete DP during power shift based on the clutch activation. Since the clutch is a nonlinear system with hysteresis, the control effectiveness could not be guaranteed. In [27], [28], the engine output torque was utilized to damp the driveline oscillations actively through an LQR control. Due to the low control accuracy of the engine, an admissible control effectiveness could not be guaranteed. In the 3DHT, an MG2 is located at the final drive ring gear with a fast response time and a high control accuracy, which can be employed as a damper to suppress the driveline oscillations.

In order to solve the mentioned problems, a novel power shift strategy is proposed to achieve coordinated torque control for the MG1, MG2, and engine, which leads to a fast and smooth shift for the 3DHT. The main contributions of this paper are summarized below:

1. In order to achieve a shift without torque interruption, a finite-time LQR is proposed to smoothly transfer torque and suppress driveline oscillations during the torque transfer process. In this process, the engine output torque tracks the reference torque while the MG2 acts like a damper to suppress the oscillations in the driveline.
2. In order to simplify the clutch's control requirements, a predictive SMC is proposed to track the sleeve speed quickly and precisely during the synchronization process.
3. A novel power shift strategy is proposed based on the 3DHT structure to improve the drivability.

This paper is organized as follows. Section II presents the powertrain system and control requirements. Section III designs a novel control strategy for power shift. Section IV presents the simulation results and a discussion. Finally, Section V includes the conclusions.

II. POWERTRAIN SYSTEM AND CONTROL REQUIREMENTS

Fig. 1 shows a schematic of the 3DHT system. The engine and MG1 are arranged before the clutch, the fixed gears of 1st gear, 2nd gear, and 3rd gear are located on the input shaft, and the loose gears and synchronizers are located on the output shaft. MG2 is connected with the ring gear of the final drive at the output shaft.

A. DYNAMIC MODEL OF THE 3DHT

The dynamic model of the 3DHT can be simplified as an integrated multi-degree of freedom system with the side shaft being a spring-damper system as shown in Fig. 2.

The engine and MG2 torque output through the final drive ring gear to the side shaft can be expressed by a torque balance

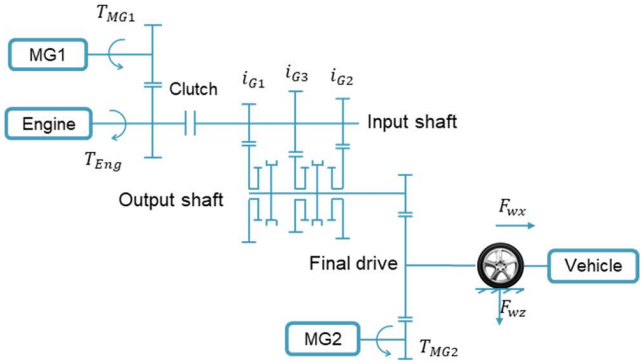

FIGURE 1. 3DHT schematic diagram.

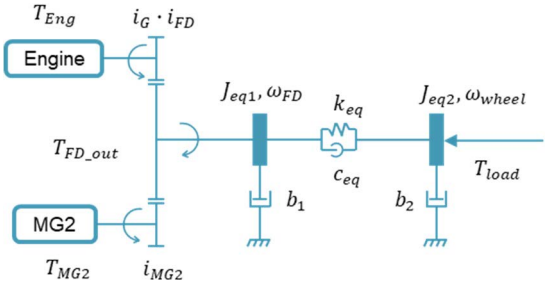

FIGURE 2. Simplified driveline model.

equation as follows:

$$T_{Eng} i_G i_{FD} + T_{MG2} i_{MG2} - J_{eq1} \dot{\omega}_{FD} - b_1 \omega_{FD} = T_{sf} \quad (1)$$

where T_{Eng}, T_{MG2}, and T_{sf} are the engine output, MG2 output, and side shaft torque, respectively. i_G, i_{FD}, and i_{MG2} are the ratios of the current gear, final drive, and MG2, respectively. ω_{FD} is the angular speed of the final drive ring gear, and b_1 is the equivalent viscous damping of the driveline before the side shaft. J_{eq1} is the equivalent inertia of the driveline before the side shaft, which can be expressed as follows:

$$J_{eq1} = \left[\left(J_{eng} + J_{ins} + J_{MG1} i_{MG1}^2\right) i_G^2 + J_{os}\right] i_{FD}^2 + J_{MG2} i_{MG2}^2 + J_{FD} \quad (2)$$

where J_{eng}, J_{ins}, J_{MG1}, J_{os}, J_{MG2}, and J_{FD} are the inertias of the engine, input shaft, MG1, output shaft, MG2, and final drive ring gear, respectively.

Since the side shaft is considered as a spring-damper system, the torsional torque, accounting for torsional compliance, can be expressed as follows:

$$T_{sf} = k_{eq} \left(\theta_{FD} - \theta_{wheel}\right) + c_{eq} \left(\omega_{FD} - \omega_{wheel}\right) \quad (3)$$

where k_{eq} and c_{eq} are the torsional stiffness and damping coefficient of the side shaft, respectively, $\theta_{FD} - \theta_{wheel}$ is the torsional angle of the side shaft, and ω_{wheel} is the angular speed of the wheel.

The torque balance equation between the side shaft and the wheel can be expressed as follows:

$$T_{sf} = T_{load} + J_{eq2} \dot{\omega}_{wheel} + b_2 \omega_{wheel} \quad (4)$$

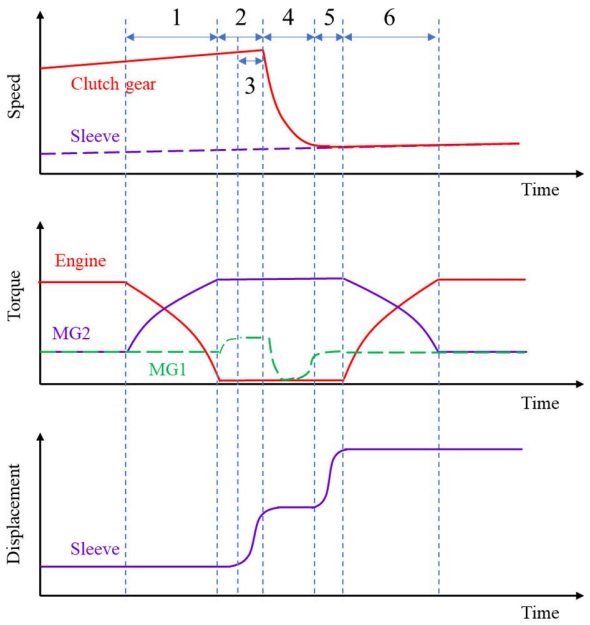

FIGURE 3. Schematic of power shift.

where b_2 is the viscous damping of the wheel, and T_{load} is vehicle load, J_{eq2} is the equivalent inertia at the wheel, which can be expressed as follows:

$$J_{eq2} = J_{wheel} + mr^2 \tag{5}$$

where J_{wheel} is the inertia of the wheel, m is the vehicle mass, and r is the tire rolling radius.

The vehicle load can be expressed as follows:

$$T_{load} = r\left(\rho A c_d v^2/2 + mgfcos\varphi + mgsin\varphi + ma\right) \tag{6}$$

where ρ is the air density, A is the equivalent front area of the vehicle, c_d is the aerodynamic resistance coefficient, v is the vehicle velocity, f is the rolling resistance coefficient, and φ is the road gradient angle, a is the vehicle acceleration.

B. CONTROL REQUIREMENT

According to the 3DHT structure, a shifting process without clutch actuation can be implemented, which is beneficial for simplifying the control requirement and extending the clutch's service life. The current gear is the first gear, and the clutch is engaged, taking the power upshift from the first gear to the second one as an example. The driving torque at the wheel is supplied only by the engine. Fig. 3 shows a schematic of the entire shift process, which is divided into six stages:

1. Torque transfer: After receiving an upshift command from the TCU, the engine output torque drops to 0Nm within a specified time, and MG2 simultaneously increases from 0Nm to the target torque to maintain a constant driving torque for the wheel.
2. Coast torque elimination: The engine enters into a coast state and generates a coast torque after completing stage 1. Since the clutch remains engaged, the engine's coast torque increases the drag torque at the input shaft, resulting in a large shifting force that disengages the sleeve from the clutch gear. Therefore, the drag torque of the input shaft should be eliminated by MG1.
3. Disengagement: The shift fork provides the shifting force required to disengage the sleeve from the active clutch gear. After disengagement, the shift fork continues to move the sleeve towards the neutral position. After that, the sleeve stops moving forward and awaits speed regulation by the target clutch gear.
4. MG1 synchronization: When the sleeve arrives at the neutral position, MG1 actively regulates the clutch gear to reduce the difference in speed between the clutch gear and the sleeve to a value lower than a particular range.
5. Engagement: The shift actuator continues to push the sleeve forward towards the target gear. After the sleeve passes the edge of the tooth, it engages with the clutch gear.
6. Similar to stage 1, the output torque at the wheel is transferred from the MG2 to the engine.

There are many indicators available for evaluating the quality of the shifting process, such as shifting time, jerk amplitude, interior noise level, and acceleration characteristics. Previous studies have found that jerk and shifting time play a decisive role in shift quality [33]–[36]. The control requirements of this study are fast shift time, low jerk, and smooth output torque at the wheel. Therefore, stages 1, 4, and 6 are the main stages that need to be studied for analyzing the shifting process of the 3DHT. In stage 1, the control objective is to maintain the output torque at the wheel constant and minimize oscillations in the driveline during torque transfer. In stage 4, for active speed synchronization, the control objective is to regulate the clutch gear to track the speed of the sleeve quickly and precisely. In stage 6, driveline systems may oscillate due to gear engagement of stage 5. The control objectives are to suppress driveline oscillations and smoothen torque changes at the wheel.

III. CONTROL DESIGN

Considering the power upshift with a constant pedal position as an example, a strategy of power shift has been developed in this study. The entire shift process is divided into six stages. As discussed in section 2, the quality of the shifting process depends heavily on stages 1, 4, and 6; hence, these stages are studied in detail.

A. TORQUE TRANSFER (STAGE 1)

1) COORDINATED TORQUE CONTROLLER DESIGN

As the engine desired output torque drops to 0Nm within a specified time, MG2 simultaneously increases the desired output torque from 0Nm to the target torque. The torque transfer process should maintain a constant drive torque at the wheel. At the end of this process, the desired torque for the MG2 can be expressed as follows:

$$T_{MG2Des} = T^r_{MG2} = T_{DriDes}/i_{MG2} \tag{7}$$

where T_{MG2Des}, T^r_{MG2}, and T_{DriDes} are the desired MG2, reference MG2, and desired driver torque at the wheel, respectively.

During the torque transfer process, the torque response time of the engine is much longer than that of MG2, and the torque control accuracy of the engine is also very low. There is always some deviation of the actual engine output torque from the desired engine output torque. Consequently, the output torque of the powertrain may fluctuate during the torque transfer process, which in turn causes longitudinal jerk of the vehicle that affects driving performance. Therefore, a coordinated optimal torque control strategy between the engine and MG2 is proposed to resolve this problem based on a finite-time LQR method.

According to (1)-(6), the state function of the torque transfer process can be expressed as follows:

$$\boldsymbol{x_a} = [x_1, x_2, x_3]^T = \left[\theta_{FD} - \theta_{wheel}, \dot{\theta}_{FD}, \dot{\theta}_{wheel}\right]^T \quad (8)$$
$$\dot{x}_1 = x_2 - x_3 \quad (9)$$
$$\dot{x}_2 = 1/J_{eq1} \cdot (T_{Eng} \cdot i_t + T_{MG2} \cdot i_{MG2} - k_{eq} \cdot x_1 - c_{eq} \cdot x_2 + c_{eq} \cdot x_3 - b_1 \cdot x_2) \quad (10)$$
$$\dot{x}_3 = 1/J_{eq2} \cdot (k_{eq} \cdot x_1 + c_{eq} \cdot x_2 - c_{eq} \cdot x_3 - b_2 \cdot x_3 - T_{load}) \quad (11)$$
$$y = T_{sf} = k_{eq} \cdot x_1 + c_{eq} \cdot x_2 - c_{eq} \cdot x_3 \quad (12)$$

The linear time-invariant state equation can be written as:

$$\dot{\boldsymbol{x}}_{\boldsymbol{a}} = \boldsymbol{A}\boldsymbol{x}_{\boldsymbol{a}} + \mathbf{B}\boldsymbol{u}_{\boldsymbol{a}} + \boldsymbol{h} \quad (13)$$
$$\boldsymbol{y}_{\boldsymbol{a}} = \boldsymbol{C}\boldsymbol{x}_{\boldsymbol{a}} \quad (14)$$

where

$$\boldsymbol{A} = \begin{bmatrix} 0 & 1 & -1 \\ -k_{eq}/J_{eq1} & -\left(c_{eq}+b_1\right)/J_{eq1} & c_{eq}/J_{eq1} \\ k_{eq}/J_{eq2} & c_{eq}/J_{eq2} & -\left(c_{eq}+b_2\right)/J_{eq2} \end{bmatrix},$$
$$\mathbf{B} = \begin{bmatrix} 0 & 0 \\ i_t/J_{eq1} & i_{MG2}/J_{eq1} \\ 0 & 0 \end{bmatrix},$$
$$\boldsymbol{u_a} = \begin{bmatrix} T_{Eng} & T_{MG2} \end{bmatrix}^T,$$
$$\boldsymbol{h} = \begin{bmatrix} 0 & 0 & -T_{load}/J_{eq2} \end{bmatrix}^T,$$
$$\boldsymbol{C} = \begin{bmatrix} k_{eq} & c_{eq} & -c_{eq} \end{bmatrix}.$$

The control objectives focus on transferring torque and suppressing driveline oscillations to improve driving quality. This implies that not only must the engine and MG2 output torque approach the reference torque $\left[T^r_{Eng}, T^r_{MG2}\right]$ asymptotically, but also the time derivative of the side shaft torque $\dot{T}_{sf}$ needs to be regulated down to zero. Therefore, the $\dot{T}_{sf}$ is defined as the output of the state space model. To ensure that the engine and MG2 output torque asymptotically follow the corresponding reference torque $\left[T^r_{Eng}, T^r_{MG2}\right]$, two more states, x_4 and x_5 are introduced. The new states x_4 and x_5 integrate the differences between reference torque and controller output torque as follows:

$$\dot{\boldsymbol{x}}_{\boldsymbol{u}} = \begin{bmatrix} \dot{x}_4 & \dot{x}_5 \end{bmatrix}^{\boldsymbol{T}} = \begin{bmatrix} T_{Eng} - T^r_{Eng} & T_{MG2} - T^r_{MG2} \end{bmatrix}^{\boldsymbol{T}} = \boldsymbol{u_a} - \boldsymbol{u^r_a} \quad (15)$$

The time derivative of the side shaft torque $\dot{T}_{sf}$ is given by:

$$\dot{T}_{sf} = \dot{\boldsymbol{y}}_{\boldsymbol{a}} = \boldsymbol{C}\dot{\boldsymbol{x}}_{\boldsymbol{a}} = \boldsymbol{C}(\boldsymbol{A}\boldsymbol{x}_{\boldsymbol{a}} + \mathbf{B}\boldsymbol{u}_{\boldsymbol{a}} + \boldsymbol{h}) \quad (16)$$

The steady solution $\boldsymbol{x^r_a}$ is defined as follows:

$$\dot{\boldsymbol{x}}^{\boldsymbol{r}}_{\boldsymbol{a}} = \boldsymbol{A}\boldsymbol{x}^{\boldsymbol{r}}_{\boldsymbol{a}} + \mathbf{B}\boldsymbol{u}^{\boldsymbol{r}}_{\boldsymbol{a}} + \boldsymbol{h} = \mathbf{0} \quad (17)$$
$$\Longrightarrow \boldsymbol{x}^{\boldsymbol{r}}_{\boldsymbol{a}} = -\boldsymbol{A}^{-\mathbf{1}}\left(\mathbf{B}\boldsymbol{u}^{\boldsymbol{r}}_{\boldsymbol{a}} + \boldsymbol{h}\right) \quad (18)$$

According to (16)-(18), the time derivative of the side shaft torque $\dot{T}_{sf}$ can be rewritten as follows:

$$\begin{aligned} \dot{T}_{sf} &= \boldsymbol{C}\left[\boldsymbol{A}\boldsymbol{x}_{\boldsymbol{a}} + \mathbf{B}\boldsymbol{u}_{\boldsymbol{a}} + \boldsymbol{h} - \left(\boldsymbol{A}\boldsymbol{x}^{\boldsymbol{r}}_{\boldsymbol{a}} + \mathbf{B}\boldsymbol{u}^{\boldsymbol{r}}_{\boldsymbol{a}} + \boldsymbol{h}\right)\right] \\ &= \boldsymbol{C}\boldsymbol{A}\left(\boldsymbol{x}_{\boldsymbol{a}} - \boldsymbol{x}^{\boldsymbol{r}}_{\boldsymbol{a}}\right) + \boldsymbol{C}\boldsymbol{B}(\boldsymbol{u}_{\boldsymbol{a}} - \boldsymbol{u}^{\boldsymbol{r}}_{\boldsymbol{a}}) \end{aligned} \quad (19)$$

Combining (13), (14), (15), (17), and (19), the linear time-invariant state equations can be rewritten as follows:

$$\dot{\bar{\boldsymbol{x}}} = \begin{bmatrix} \dot{\boldsymbol{x}}_{\boldsymbol{a}} \\ \dot{\boldsymbol{x}}_{\boldsymbol{u}} \end{bmatrix} = \begin{bmatrix} \boldsymbol{A} & \mathbf{0} \\ \mathbf{0} & \mathbf{0} \end{bmatrix} \begin{bmatrix} \boldsymbol{x}_{\boldsymbol{a}} - \boldsymbol{x}^{\boldsymbol{r}}_{\boldsymbol{a}} \\ \boldsymbol{x}_{\boldsymbol{u}} \end{bmatrix} + \begin{bmatrix} \mathbf{B} \\ \mathbf{1} \end{bmatrix} \left(\boldsymbol{u}_{\boldsymbol{a}} - \boldsymbol{u}^{\boldsymbol{r}}_{\boldsymbol{a}}\right) = \bar{\boldsymbol{A}}\bar{\boldsymbol{x}} + \bar{\boldsymbol{B}}\dot{\boldsymbol{u}} \quad (20)$$

$$\bar{\mathbf{y}} = \begin{bmatrix} \dot{T}_{sf} \\ \boldsymbol{x}_{\boldsymbol{u}} \end{bmatrix} = \begin{bmatrix} \boldsymbol{C}\boldsymbol{A} & \mathbf{0} \\ \mathbf{0} & \mathbf{1} \end{bmatrix} \begin{bmatrix} \boldsymbol{x}_{\boldsymbol{a}} - \boldsymbol{x}^{\boldsymbol{r}}_{\boldsymbol{a}} \\ \boldsymbol{x}_{\boldsymbol{u}} \end{bmatrix} + \begin{bmatrix} \boldsymbol{C}\boldsymbol{B} \\ \mathbf{0} \end{bmatrix} \left(\boldsymbol{u}_{\boldsymbol{a}} - \boldsymbol{u}^{\boldsymbol{r}}_{\boldsymbol{a}}\right) = \bar{\boldsymbol{C}}\bar{\boldsymbol{x}} + \bar{\boldsymbol{D}}\dot{\boldsymbol{u}} \quad (21)$$

The cost function for the finite-time LQR should always contain the control signals which balance performance and control effort. To achieve a better driving quality the $\dot{T}_{sf}$ should be minimized. Besides, during this stage, the engine and MG2 output torque must approach the reference torque $\boldsymbol{u^r_a}$ asymptotically within a specified time. Therefore, the cost function for the LQR controller can be expressed as follows:

$$\begin{aligned} J &= \frac{1}{2}\bar{\mathbf{y}}^{\boldsymbol{T}}\left(t_f\right)\boldsymbol{S}\bar{\mathbf{y}}\left(t_f\right) + \frac{1}{2}\int_{t_0}^{t_f} \bar{\mathbf{y}}^{\boldsymbol{T}}\boldsymbol{Q}\bar{\mathbf{y}} + \dot{\boldsymbol{u}}^{\boldsymbol{T}}\boldsymbol{R}\dot{\boldsymbol{u}}\boldsymbol{dt} \\ &= \frac{1}{2}\bar{\mathbf{y}}^{\boldsymbol{T}}\left(t_f\right)\boldsymbol{S}\bar{\mathbf{y}}\left(t_f\right) + \frac{1}{2}\int_{t_0}^{t_f} \begin{bmatrix} \bar{\boldsymbol{x}}^T & \dot{\boldsymbol{u}}^T \end{bmatrix} \times \begin{bmatrix} \bar{\boldsymbol{Q}} & \boldsymbol{M} \\ \boldsymbol{M}^{\boldsymbol{T}} & \bar{\boldsymbol{R}} \end{bmatrix} \begin{bmatrix} \bar{\boldsymbol{x}} \\ \bar{\boldsymbol{u}} \end{bmatrix} \boldsymbol{dt} \end{aligned} \quad (22)$$

where $\bar{\boldsymbol{Q}} = \bar{\mathbf{C}}^{\boldsymbol{T}}\boldsymbol{Q}\bar{\mathbf{C}}$, $\boldsymbol{M} = \bar{\mathbf{C}}^{\boldsymbol{T}}\boldsymbol{Q}\bar{\boldsymbol{D}}$, $\bar{R} = \bar{D}^{\boldsymbol{T}}\boldsymbol{Q}\bar{\boldsymbol{D}} + \boldsymbol{R}$. It is worth noting that the torque control accuracy of the MG2 is higher than that of the engine, and the torque response is also faster. The MG2 should therefore take on the main role of suppressing oscillations of the driveline. Therefore, the weighting factor $\boldsymbol{R}$ (1, 1) should much larger than $\boldsymbol{R}$ (2, 2).

The optimal control problem can be solved by using a matrix differential Riccati equation.

$$\dot{\boldsymbol{P}}\left(t\right) = -\boldsymbol{P}\left(t\right)\bar{\boldsymbol{A}} - \bar{\boldsymbol{A}}^{\boldsymbol{T}}\boldsymbol{P}\left(t\right) - \bar{\boldsymbol{Q}} + \left(\boldsymbol{P}\left(t\right)\bar{\boldsymbol{B}} + \boldsymbol{M}\right)\bar{R}^{-1}\left(\bar{\boldsymbol{B}}^{\boldsymbol{T}}\boldsymbol{P}\left(t\right) + \boldsymbol{M}^{\boldsymbol{T}}\right) \quad (23)$$

$$\boldsymbol{K}\left(t\right) = \bar{R}^{-1}\left(\bar{\boldsymbol{B}}^{\boldsymbol{T}}\boldsymbol{P}\left(t\right) + \boldsymbol{M}^{\boldsymbol{T}}\right) \quad (24)$$

$$\boldsymbol{K}\left(t\right)_{(2\times5)} = \left[\boldsymbol{K}\left(t\right)_{\boldsymbol{a}(2\times3)}\boldsymbol{K}\left(t\right)_{\boldsymbol{u}(2\times2)}\right] \quad (25)$$

The terminal condition is $\boldsymbol{P}\left(t_f\right) = \boldsymbol{S}\left(t_f\right)$. The $\boldsymbol{P}\left(\boldsymbol{t}\right)$ is calculated offline and stored in a lookup table which can

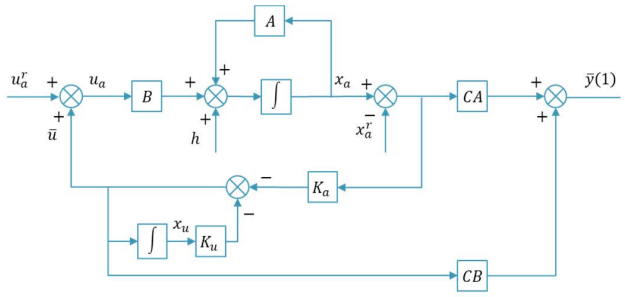

FIGURE 4. LQR control structure.

be read online. A state feedback control relationship can be expressed as follows:

$$\dot{\boldsymbol{u}} = -\boldsymbol{K}(t)\bar{\boldsymbol{x}} = -\boldsymbol{K}(t)_a\left(\boldsymbol{x_a} - \boldsymbol{x_a^r}\right) - \boldsymbol{K}(t)_u\boldsymbol{x_u} \quad (26)$$

$$\boldsymbol{u_a} = \dot{\boldsymbol{u}} + \boldsymbol{u_a^r} \quad (27)$$

The LQR control structure for the torque transfer process is shown in Fig. 4.

2) OBSERVER DESIGN

The finite-time LQR is a state feedback control that requires full state vector information. However, not all states are available in the driveline system. The speed of the final drive ring gear can be obtained by the speed sensor of MG2. The wheel speed can also be measured through the wheel speed sensor although with a low resolution. In addition, the side shaft torque requires an additional torque sensor, which increases the cost of the vehicle. Therefore, to control cost and reduce the error due to the accuracy of the sensor, a state observer is introduced in the expression for control. The measured speed of the MG2 is the only measurement used as an input to the observer. A Kalman filter is proposed to estimate the states of the wheel speed and side shaft torque.

According to (13), the discrete system function can be expressed as follows:

$$\boldsymbol{x_a}(k+1) = (\boldsymbol{I} + T_K\boldsymbol{A})\boldsymbol{x_a}(k) + T_K\mathbf{B}\boldsymbol{u_a} + T_K\boldsymbol{h} \quad (28)$$

where T_K is the system sample time.

Selecting the speed of the final drive ring gear as the measurement signal, and the measurement matrix as $\boldsymbol{H} = [0\ 1\ 0]$. Equation (28) can be rewritten as the following form:

$$\boldsymbol{x_a}(k) = \tilde{\boldsymbol{A}}\boldsymbol{x_a}(k-1) + \tilde{\boldsymbol{B}}\boldsymbol{u_a} + T_K\boldsymbol{h} + \boldsymbol{w}(k-1) \quad (29)$$

$$\boldsymbol{z}(k) = \boldsymbol{H}\boldsymbol{x_a}(k-1) + \boldsymbol{v}(k-1) \quad (30)$$

where $\tilde{\boldsymbol{A}} = \boldsymbol{I} + T_K\boldsymbol{A}$, $\tilde{\boldsymbol{B}} = T_K\boldsymbol{B}$, and $\boldsymbol{w}(k) = \left[w_1(k)\ w_2(k)\ w_3(k)\right]^T$. $w_1(k)$, $w_2(k)$, and $w_3(k)$ are the process noises, and $\boldsymbol{v}(k)$ is the measurement noise. These noises are considered as Gaussian white noises whose expected values are zero and covariance matrices are $\boldsymbol{Q}$ and $\boldsymbol{R}$.

The iterative algorithm of the Kaman filter is expressed as follows:

$$\hat{\boldsymbol{x}}_a^-(k) = \tilde{\boldsymbol{A}}\hat{\boldsymbol{x}}_a(k-1) + \tilde{\boldsymbol{B}}\boldsymbol{u_a} + T_K\boldsymbol{h} \quad (31)$$

$$\boldsymbol{P}^-(k) = \tilde{\boldsymbol{A}}\boldsymbol{P}^-(k-1)\tilde{\boldsymbol{A}}^T + \boldsymbol{Q} \quad (32)$$

The optimal Kalman gain $\boldsymbol{K}(k)$ can be calculated by the unbiased and minimum variance criteria:

$$\boldsymbol{K}(k) = \boldsymbol{P}^-(k)\boldsymbol{H}^T\left[\boldsymbol{H}\boldsymbol{P}^-(k)\boldsymbol{H}^T + \boldsymbol{R}\right]^{-1} \quad (33)$$

$$\hat{\boldsymbol{x}}_a(k) = \hat{\boldsymbol{x}}_a^-(k) + \boldsymbol{K}(k)\left[\boldsymbol{z}(k) - \boldsymbol{H}\hat{\boldsymbol{x}}_a^-(k)\right] \quad (34)$$

$$\boldsymbol{P}(k) = [\boldsymbol{I} - \boldsymbol{K}(k)\boldsymbol{H}]\boldsymbol{P}^-(k) \quad (35)$$

where $\hat{\boldsymbol{x}}_a^-$ is a priori state estimate, $\boldsymbol{P}^-$ is a priori error covariance matrix, $\hat{\boldsymbol{x}}_a$ is a posteriori state estimate, and $\boldsymbol{P}$ is a posteriori error covariance matrix.

According to (12), the estimate of the side shaft torque can be express as follows:

$$\hat{T}_{sf}(k) = \boldsymbol{C}\hat{\boldsymbol{x}}_a(k) \quad (36)$$

The Kalman Filter runs when the vehicle starts and continues running after the vehicle starts.

B. COAST TORQUE ELIMINATION (STAGE 2)

The engine enters a coast state and generates a coast torque after the completion of stage 1. The clutch remains engaged, hence the coast torque of the engine increases the drag torque at the input shaft. If the drag torque on the input shaft is large, it results in a large shifting force that disengages the sleeve and the clutch gear. Therefore, the drag torque of the input shaft should be eliminated. MG1 operates in a torque open loop mode to eliminate the drag torque of the input shaft.

C. DISENGAGEMENT (STAGE 3)

The shift fork provides the shifting force needed to disengage the sleeve from the active clutch gear. After disengagement, the shift fork continues to move the sleeve to the neutral position. The sleeve then stops moving forward and awaits speed regulation by the MG1. The shift actuator is in a velocity closed-loop and a position closed loop. The control at this stage has very little impact on shift quality. Therefore, a conventional PI controller is applied in this stage.

D. MG1 SYNCHRONIZATION (STAGE 4)

During this process, the time consumed by synchronization and the speed difference at the end of this process have a significant effect on the shifting quality. This is because, at the end of this stage, a speed difference can result in large frictional work during mechanical synchronization in stage 5, as a consequence of the very large inertia of the input shaft. Therefore, it is necessary to quickly regulate the speed difference between the clutch gear and sleeve, and precisely track the speed of the sleeve. A predictive SMC is proposed which has the advantages of fast response, and insensitivity to parameter changes and external disturbances. The speed synchronization process can be expressed as a linear time-invariant, single-input, single-output system, and the simplified system structure is as shown in Fig. 5.

$$\dot{x} = bu(t) + f + d \quad (37)$$

where $\dot{x} = \dot{\omega}_{clu}$, $b = 1/\left(J_{eq3}i_G\right)$, $f = -T_f\left(\dot{\theta}_{eng}, t_{eng}\right)/\left(J_{eq}i_G\right)$, and $u(t) = T_{MG1}i_{MG1}$. $\dot{\omega}_{clu}$ is the angular

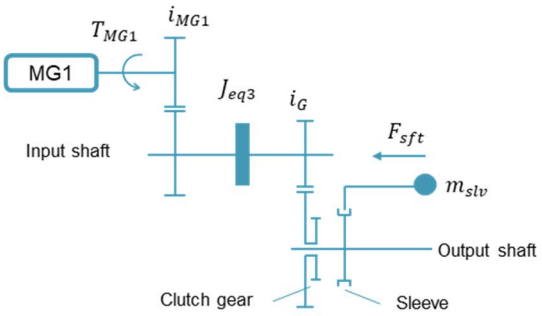

FIGURE 5. Simplified model of the driveline.

acceleration of the clutch gear, J_{eq3} is the equivalent inertia of the input shaft, and d is the external disturbance.

The tracking error and sliding function are defined as follows:

$$e(t) = x(t) - x_d(t) \tag{38}$$

$$s(t) = e(t) + c\int_0^t e(t)\,dt \tag{39}$$

where $x_d(t) = \omega_{slv}$, ω_{slv} is the angular velocity of the sleeve, and c is a constant greater than 0.

It is predicted that the sliding surface after a predictive period T_S can be expressed as follows:

$$s(t + T_S) = s(t) + T_S\dot{s}(t) \tag{40}$$

The predictive control target is $s(t + T_S) \rightarrow 0$, that is, $x(t + T_S) \rightarrow x_d(t + T_S)$.

The cost function of SMC can be expressed as follows [37]:

$$J(x, u, t) = s^2(t + T_S)/2 \tag{41}$$

To achieve optimal control, the following condition must be met:

$$\frac{\partial J(x, u, t)}{\partial u} = s(t + T_S)\frac{\partial s(t + T_S)}{\partial u} = 0 \tag{42}$$

Since,

$$\begin{aligned}\frac{\partial s(t + T)}{\partial u} &= \frac{\partial(s(t) + T\dot{s}(t))}{\partial u} \\ &= T_S\frac{\partial(bu(t) + f + d - \dot{x}_d(t))}{\partial u} = bT_S\end{aligned} \tag{43}$$

The optimal control condition is then transformed into the following equation:

$$s(t + T_S) = 0 \tag{44}$$

Combining (37)-(40), and (44) yields the expression for control as:

$$u = (-ce + \dot{x}_d - f - s/T_S - d)/b \tag{45}$$

The tracking problem is to find an expression for control $u(t)$ such that the state $x(t)$ can approach and remain on the sliding surface. To prevent system chattering due to the system state frequently passing through the sliding surface when the system state is close to this surface, the external disturbance d can be replaced by $Dsat(s)$, where $|d| \leq D$. $sat(s)$ is a saturation function, which can be expressed as follows:

$$sat(s) = \begin{cases} 1 & s > \Delta \\ s/\Delta & |s| \leq \Delta \\ -1 & s < \Delta \end{cases} \tag{46}$$

where Δ is the width of the boundary layer of the sliding surface.

To verify the stability of the controller, a Lyapunov function is defined as follows:

$$V = s^2/2 \tag{47}$$

Combining (40), (44), and (47) yields the expression of $\dot{V}$ as:

$$\dot{V} = s\dot{s} = -s^2/T_S = -2V/T_S \tag{48}$$

The solution of $\dot{V} = -2V/T_S$ is:

$$V(t) = e^{-\frac{2}{T_S}(t - t_0)}V(t_0) \tag{49}$$

It is apparent that $V(t)$ and s converge to 0 exponentially, hence, e and $\int_0^t edt$ also converge to 0 exponentially, so that the system is stable. Besides, the smaller the T_S, the faster the approaching speed of the system.

E. ENGAGEMENT (STAGE 5)

After speed synchronization, the shift actuator continues to push the sleeve forward towards the target gear. After the sleeve passes the edge of the tooth, the sleeve and the clutch gear are engaged. The shift actuator is in the shifting force open-loop mode. A constant shift force is applied on the shift fork until the sleeve passes the edge.

F. TORQUE TRANSFER (STAGE 6)

The MG2 output torque drops to 0Nm within the specified time. The output torque of the engine simultaneously increases from 0Nm to the target torque. After the engagement, the impact between the clutch gear and sleeve causes oscillations in the driveline system. Besides, since the active gear has shifted to the upper gear, the output torque at the wheel drops during the torque transfer. Consequently, the angular acceleration will change within a short time which could amplify the oscillations and result in poor driving quality. The finite-time LQR proposed in stage 1 is also suitable for this stage which could suppress the oscillations and transfer torque smoothly.

The entire shifting process concludes after the completion of stage 6, and the control structure diagram is shown in Fig. 6.

IV. SIMULATION RESULTS AND DISCUSSION

In order to verify the proposed power shift strategy, a simulation model is established with the Matlab/Simulink based on the mentioned mathematical models. The Simulink/Simscape and Simulink/Stateflow modules are employed for powertrain modeling and control strategy modeling, respectively. A fixed-step Euler solver is selected to compute the model states within a 1ms sample time. Table 1 presents the main input parameters of the simulation model.

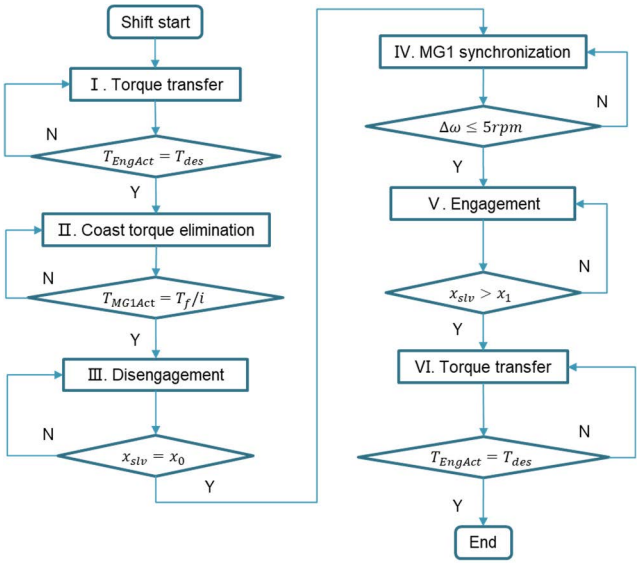

FIGURE 6. Control diagram of power shift.

TABLE 1. Model input parameters.

Parameters	Value	Unit
Vehicle mass	1920	*kg*
Tire rolling radius	0.348	*m*
Vehicle front area	2.75	m^2
Air resistance coefficient	0.32	-
Rolling resistance coefficient	0.009	-
MG1 nominal torque	60	*Nm*
MG2 nominal torque	270	*Nm*
Engine nominal torque	250	*Nm*
1st gear ratio	1.515	-
2nd gear ratio	0.977	-
3rd gear ratio	0.633	-
MG1 gear ratio	2.31	-
MG2 gear ratio	2.52	-
FD gear ratio	4.647	-

A. COORDINATED TORQUE CONTROL

In order to evaluate the effectiveness of the proposed coordinated torque control, a torque feedforward control is introduced. In the torque feedforward control, the desired output torque of the engine and motor increases and decreases linearly, respectively. The controller aims to keep the desired output torque at the wheel unchanged. However, the response time of MG2 is faster than that of the engine, and the control accuracy of the engine is low. Since there is no feedback control, the driveline system may oscillate in the torque transfer process. Besides, to better observe the effectiveness of the proposed method, the torque transfer process after gear engagement is taken as the comparison target because the driveline begins to oscillate after gear engagement. If the coordinated torque control works poorly, the system oscillations may be amplified. It is assumed that these two methods have the same simulation curves before the torque transfer process, while different methods are only applied at the beginning of the torque transfer process.

Fig. 7 shows stage 6 of a power shift process from the second gear to the third one, i.e., the torque transfer process. It is an engagement process before 1.57s, generating a jerk around -4 m/s^3 due to the clutch gear and sleeve interaction, as shown in Fig. 7(b). After 1.57s, the system enters the torque transfer process. The wheel torque fluctuates due to the interaction in the previous stage. Therefore, the proposed LQR-based active damping controller suppresses oscillations by regulating the desired output torque of the engine and MG2. The control accuracy cannot be guaranteed since the engine output torque is affected by altitude and intake air temperature. Besides, the engine's turbocharger behavior also led to a torque delay. However, MG2 has a higher torque control accuracy and a faster response time. It plays a significant role in alleviating the oscillations by regulating the weighting factors in the cost function of the LQR. Therefore, the oscillations can be suppressed by regulating the desired output torque of the MG2, as shown in Fig. 7(a). The MG2 acts like an active damper to suppress the oscillations actively. Since the output torque of MG2 is fluctuating, the speed of MG2 is also fluctuating, as shown in Fig. 7(c). Meanwhile, the torque transfer between the engine and MG2 should be completed within a specified time. Due to the gear being upshifted, the desired driver torque at the wheel is reduced. In Fig. 7(b), the wheel torque decreases smoothly to the target torque with a $|\boldsymbol{Jerk_{max}}| = 8$ m/s^3.

However, according to the torque feedforward control, the desired output torque of the engine and MG2 is linearly increased and decreased, respectively, to maintain the wheel torque uninterrupted, as shown in Fig. 7(a). The wheel torque fluctuates throughout the process without an active damping control, as shown in Fig. 7(b). A $|\boldsymbol{Jerk_{max}}| = 14.8$ m/s^3 occurs which is 6.8 m/s^3 higher than the LQR method.

B. ACTIVE SPEED SYNCHRONIZATION

A PID controller is introduced to verify the effectiveness of the proposed predictive SMC. In the active speed synchronization with PID control, the output torque of MG1 is selected as the input signal, and the sleeve speed is selected as the reference signal. Three sets of PID controller parameters are selected for comparison: 1) PID1, $K_p = 3$, $K_i = 0.2$, $K_d = 0$; 2) PID2, $K_p = 10$, $K_i = 0.2$, $K_d = 0$; 3) PID3, $K_p = 10$, $K_i = 0.3$, $K_d = 0$. The differential coefficient K_d is set to 0 because the differential part of the PID will change sharply under a step-change in the feedback signal caused by external disturbance, which may cause the system to be unstable.

Besides, the speed synchronization process is simulated separately better to observe the effectiveness of the proposed predictive SMC. It is assumed that the sleeve speed is 2475 rpm at the beginning of the simulation, while the clutch gear speed is 3470 rpm. The vehicle is in the coast state with the torque interrupted, and the MG1 starts to regulate the clutch gear speed at 0s, as shown in Fig. 8. In the beginning, the speed difference between the clutch gear and sleeve is

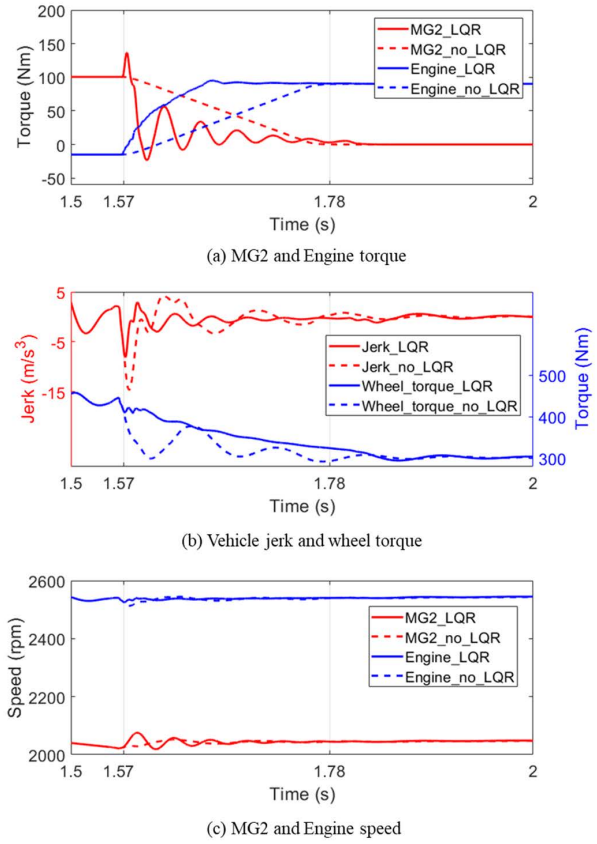

(a) MG2 and Engine torque

(b) Vehicle jerk and wheel torque

(c) MG2 and Engine speed

FIGURE 7. Simulation of torque transfer process.

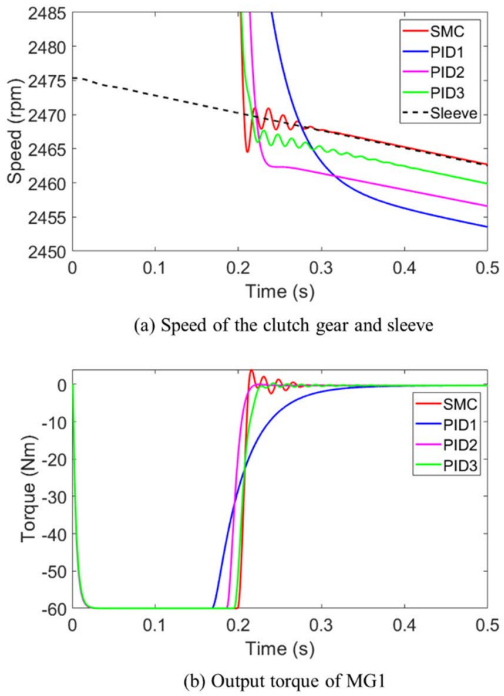

(a) Speed of the clutch gear and sleeve

(b) Output torque of MG1

FIGURE 8. Simulation of active speed synchronization process.

about 1000 rpm, and the sleeve decelerates with low deceleration due to the vehicle's coast state, as shown in Fig. 8(a).

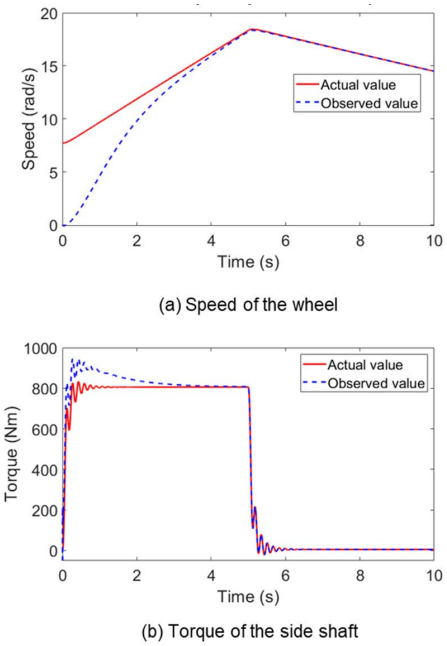

(a) Speed of the wheel

(b) Torque of the side shaft

FIGURE 9. Characteristics of the Kalman Filter.

Both the SMC and PID controllers reach the maximum output torque of the motor due to the significant speed difference at the initial stage, as shown in Fig. 8(b). At 0.22s, after the system state of the SMC crosses the sliding surface for the second time, the speed difference between the clutch gear and sleeve is within 2 rpm, and the system state runs along with the sliding surface. After 0.28s, the speed difference is almost eliminated.

However, the PID1 controller keeps the speed difference around 9 rpm after 0.38s, as shown in Fig. 8(a). This is a static error problem of the PID controller, which cannot be quickly eliminated by adjusting the integral coefficient Ki. The PID2 controller increases the Kp from 3 to 10. Therefore, the convergence time of PID2 is 0.1s faster than that of PID1. However, the static error is maintained at around 7 rpm. The PID3 controller increases the Kp from 3 to 10 and increases Ki from 0.2 to 0.3. Although the speed difference is reduced to 4 rpm after 0.22s, it is challenging to eliminate the static error of the speed difference.

C. STATE OBSERVATION

In order to verify the effectiveness of the Kalman Filter when the initial state is inconsistent with the system state, it is assumed that the vehicle accelerates with an initial velocity of 10 km/h and enters a coast state after 5s. The initial value of the Kalman Filter state is 0. Fig. 9 shows the simulation results. The observed wheel speed and side shaft torque converge to the actual value within 3.5s and then accurately track the actual value.

D. POWER SHIFT PROCESS

Fig. 10 presents the simulation results of the proposed shift control strategy for a power shift (2^{nd} -> 3^{rd}) at a vehicle velocity of 80 km/h. The speed of the sleeve is about

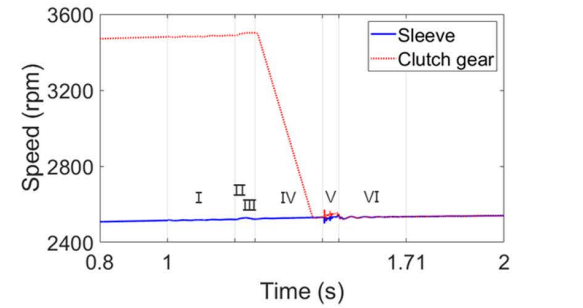

(a) Sleeve and clutch gear speed

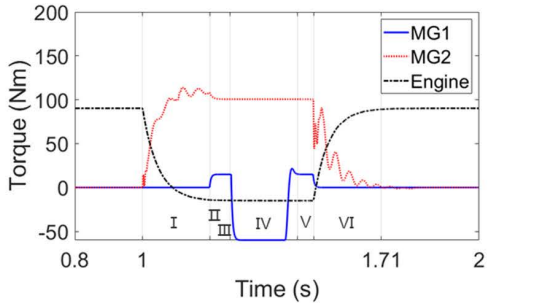

(b) MG1, MG2 & engine torque

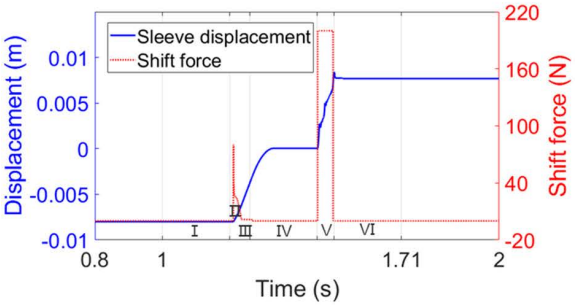

(c) Sleeve displacement and shift force

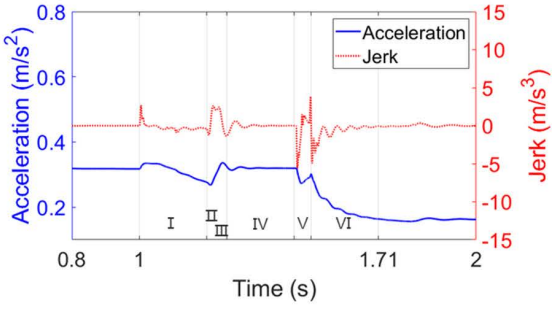

(d) Vehicle acceleration and jerk

FIGURE 10. Simulation results (2^{nd} -> 3^{rd}) of a power shift strategy with an LQR and an SMC.

2500 rpm and the speed of the target clutch gear is about 3470 rpm, as shown in Fig. 10(a). The entire shifting process is divided into six stages, over a total time of 0.71s. At 1.0s the hybrid control unit (HCU) receives an upshift request, and the shifting process enters stage 1. The output torque at the wheel is transferred from the engine to MG2 in 0.2s using the coordinated optimal torque control based on a finite time LQR, as shown in Fig. 10(b). The amplitude of the acceleration fluctuations is 0.05 m/s^2, and the jerk is maintained at a value close to zero during this stage, as shown in Fig. 10(d). After completing the torque transfer, the shifting process enters stage 2. MG1 works in a torque open loop mode to balance the coast torque of the engine. The actual engine coast torque can be interpolated from the engine friction map based on the engine speed and temperature. After the torque from MG1 replaces the coast torque of the engine, the shifting process enters stage 3. The shift actuator enters a velocity closed-loop control mode and moves the sleeve towards the neutral position, for a target velocity of 0.1 m/s. A shifting force of 80 N is required to disengage the sleeve from the clutch gear due to an undercut angle between the tooth face of the sleeve and the clutch gear, as shown in Fig. 10(c). As the sleeve disengages from the clutch gear, the shift actuator enters a distance closed-loop mode and moves the sleeve to the neutral position. When the sleeve is disengaged, the shifting process enters stage 4. MG1 works in a speed closed-loop mode based on the proposed predictive SMC, regulating the clutch gear speed and tracking the sleeve speed. The initial difference in speed between the clutch gear and the sleeve is 1000 rpm which drops to 0 rpm within 0.18s and is maintained at approximately +1 rpm, as shown in Fig. 10(a). The shifting process then enters stage 5, at which the shift actuator enters a shifting force open-loop mode. A shifting force of 200 N is applied to the sleeve to engage with the clutch gear of the 3rd gear. MG1 enters the torque open-loop mode and eliminates the coast torque of the engine. Impact occurs when the sleeve reaches the tooth surface of the clutch gear and the driveline oscillates with a maximum $|Jerk_{max}| = 5.6m/s^3$. After the sleeve crosses the edge of the clutch gear, the engagement is completed, and this process lasts 0.05s. The shifting process then enters stage 6. The output torque at the wheel is transferred from MG2 to the engine. Since the gear is upshifted, the desired driver torque at the wheel is reduced. The acceleration decreases smoothly from 0.3 m/s^2 to 0.16 m/s^2, and the oscillations of the transmission system are effectively damped to zero, as shown in Fig. 10(d). The entire shifting process is completed after the completion of stage 6. The entire shifting process lasts for 0.71s during which the driving force of the vehicle remains uninterrupted.

In order to verify the effectiveness of the proposed control algorithms, a power shift simulation without LQR and SMC is performed, as shown in Fig. 11. In stages 1 and 6, the LQR is replaced by a torque feedforward control. In stage 4, the SMC is replaced by a PI controller. In stage 1, the desired output torque of the engine and motor increases and decreases linearly, respectively, to maintain the desired torque at the wheel unchanged, as shown in Fig. 11(b). However, the actual torque response time of the engine and MG2 are different, which causes torque fluctuations in the driveline system. It can be seen that the amplitude of the acceleration fluctuations during stage 1 in Fig. 11(d) is 0.06 m/s^2 higher

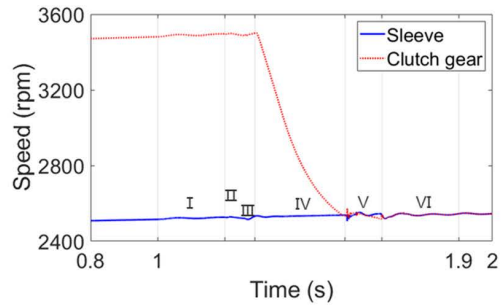

(a) Sleeve and clutch gear speed

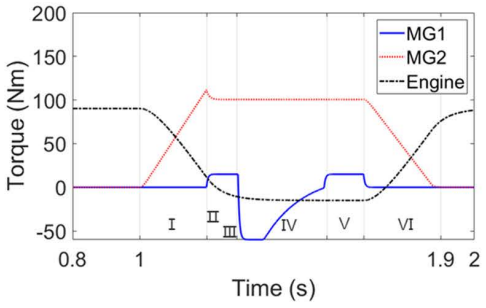

(b) MG1, MG2 & engine torque

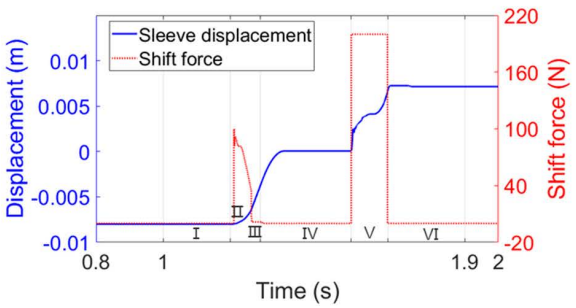

(c) Sleeve displacement and shift force

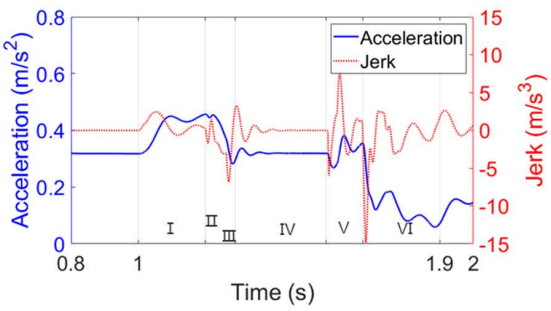

(d) Vehicle acceleration and jerk

FIGURE 11. Simulation results (2nd -> 3rd) of a power shift strategy with a feedforward control and a PI control.

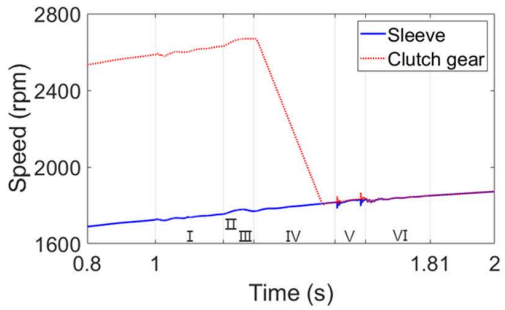

(a) Sleeve and clutch gear speed

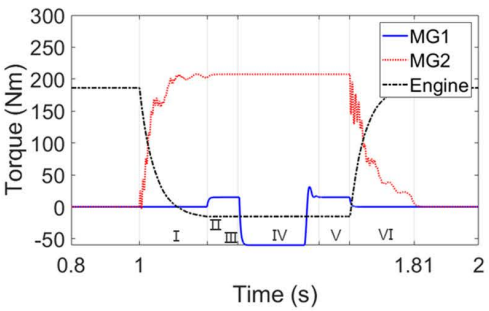

(b) MG1, MG2 & engine torque

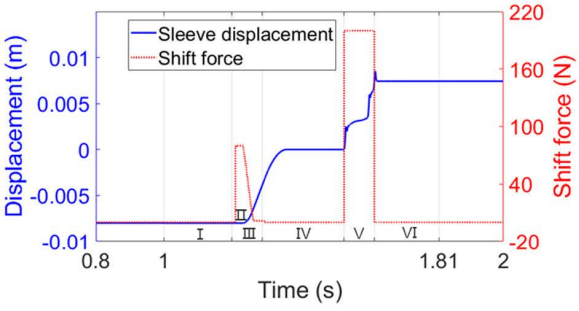

(c) Sleeve displacement and shift force

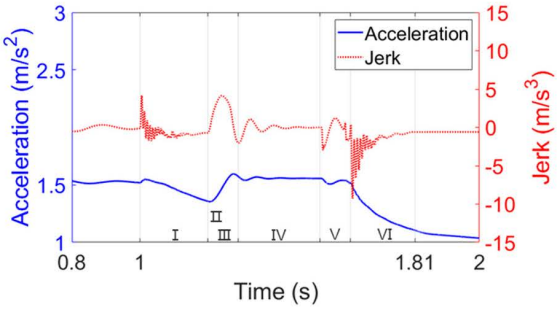

(d) Vehicle acceleration and jerk

FIGURE 12. Simulation results (1st -> 2nd) of a power shift strategy with an LQR and an SMC.

than that in Fig. 10(d). In stage 4, the controller in Fig. 11 is a PI controller. The initial difference in speed between the clutch gear and sleeve is 1000 rpm, which drops to 0 rpm within 0.27s and is maintained at approximately -6 rpm, as shown in Fig. 11(a). However, as shown in Fig. 10, it only takes 0.18s to reach the target speed, while the speed difference is maintained at approximately $+1$ rpm. It can be seen that the proposed SMC is 0.09s faster than the PI controller. In stage 6, the torque transfer process enhances the driveline oscillations due to the engagement of stage 5.

As shown in Fig. 11(d), a $|Jerk_{max}|$ of 14.8 m/s^3 occurs, 9.2 m/s^3 higher than in Fig. 10(d). Besides, the acceleration in Fig. 11(d) fluctuates throughout the process, while the acceleration in Fig. 10(d) decreases smoothly to the target acceleration. As shown in Fig. 11, the entire shifting process lasts 0.9s, which is 0.19s longer than in Fig. 10. According to the above comparisons, it indicates that the proposed power shift strategy can reduce the maximum jerk from 14.8 m/s^3 to 5.6 m/s^3, while the entire shifting time is shortened from 0.9s to 0.71s.

In order to evaluate the effectiveness of the proposed shift control strategy under different dynamic conditions, a power shift (1st -> 2nd) with a middle pedal position at a vehicle velocity of 50 km/h is presented in Fig.12. At the beginning of the shift, the speed difference between the sleeve and clutch gear is about 900 rpm which is synchronized within 0.22s, as shown in Fig. 12(a). An engine output torque of 186 Nm is requested from the driver before the shift. The output torque at the wheel is transferred in 0.2s from the engine to MG2 in stage 1, and it transfers back from MG2 to the engine in stage 6, as shown in Fig. 12(b). A $|Jerk_{max}|$ of 9.2 m/s^3 occurs as shown in Fig. 12(d). The entire shifting process takes 0.81s. According to the simulation results of Fig. 10 and Fig. 12, the proposed power shift strategy can work well with different vehicle dynamic conditions.

V. CONCLUSION

This paper studies the power shift process without the actuation of the clutch in a 3DHT. The main conclusions are drawn as follows:

1. A finite-time LQR is designed to smoothly transfer torque and suppress driveline oscillations during the torque transfer process. The engine output torque tracks the reference torque, while the MG2 actively damps the oscillations in the driveline. Comparing the simulation results with a torque feedforward control indicates that the finite-time LQR can reduce the maximum jerk by 9.2 m/s^3.
2. An active synchronization control without actuation of the clutch is studied in this paper to simplify the clutch's control requirements. A predictive SMC is designed to track the speed of the sleeve during the synchronization process. Comparing the simulation results with a PID controller indicates that the synchronization time of the predictive SMC is shortened by 0.09s, and the static error is reduced to 1rpm.
3. A power shift strategy is designed based on the 3DHT structure to improve the drivability. A comparison of the simulation result with other power shift strategy indicates that the proposed strategy can shorten the shifting time by 0.19s and alleviate the maximum jerk by 9.2 m/s^3.

In a word, the proposed power shift control strategy effectively improves the shift quality. However, there is still much room for improvement. For example, the shift force can be optimized to balance the engagement time and jerk during the engagement. An adaptive learning strategy should be designed to guarantee shift quality in the presence of parametric uncertainties and external disturbances. Moreover, a vehicle test should be performed to evaluate the performance of the proposed control strategy in the future.

ACKNOWLEDGMENT

The project is jointly completed by Nanchang University and Magna PT Powertrain (Jiangxi) Company Ltd. The authors thank Prof. Huang Juhua for her careful guidance of the research. They also thank Xu Huihui and Liu Chong for the project data. They also thank Yin Jinju and Zhang Lei for the support of the simulation.

REFERENCES

[1] S. Wang, K. Chen, F. Zhao, and H. Hao, "Technology pathways for complying with corporate average fuel consumption regulations up to 2030: A case study of China," *Appl. Energy*, vol. 241, pp. 257–277, May 2019.

[2] G. Fontaras, N.-G. Zacharof, and B. Ciuffo, "Fuel consumption and CO_2 emissions from passenger cars in Europe–laboratory versus real-world emissions," *Prog. Energy Combustion Sci.*, vol. 60, pp. 97–131, May 2017.

[3] J. T. J. Burd, E. A. Moore, H. Ezzat, R. Kirchain, and R. Roth, "Improvements in electric vehicle battery technology influence vehicle lightweighting and material substitution decisions," *Appl. Energy*, vol. 283, Feb. 2021, Art. no. 116269.

[4] R. Tan and B. Lin, "Are people willing to support the construction of charging facilities in China?" *Energy Policy*, vol. 143, Aug. 2020, Art. no. 111604.

[5] M. S. H. Lipu, M. A. Hannan, T. F. Karim, A. Hussain, M. H. M. Saad, A. Ayob, M. S. Miah, and T. M. I. Mahlia, "Intelligent algorithms and control strategies for battery management system in electric vehicles: Progress, challenges and future outlook," *J. Cleaner Prod.*, vol. 292, Apr. 2021, Art. no. 126044.

[6] M. Inci, M. Büyük, M. H. Demir, and G. Ilbey, "A review and research on fuel cell electric vehicles: Topologies, power electronic converters, energy management methods, technical challenges, marketing and future aspects," *Renew. Sustain. Energy Rev.*, vol. 137, Mar. 2021, Art. no. 110648.

[7] S. Bagheri, Y. Huang, P. D. Walker, J. L. Zhou, and N. C. Surawski, "Strategies for improving the emission performance of hybrid electric vehicles," *Sci. Total Environ.*, vol. 771, Jun. 2021, Art. no. 144901.

[8] X. Li and A. Jenn, "Energy, emissions, and cost impacts of charging price strategies for electric vehicles," *Environ. Sci. Technol.*, vol. 56, no. 9, pp. 5724–5733, Apr. 2022.

[9] W. Zhuang, S. Li Eben, X. Zhang, D. Kum, Z. Song, G. Yin, and F. Ju, "A survey of powertrain configuration studies on hybrid electric vehicles," *Appl. Energy*, vol. 262, Mar. 2020, Art. no. 114553.

[10] D.-D. Tran, M. Vafaeipour, M. E. Baghdadi, R. Barrero, J. Van Mierlo, and O. Hegazy, "Thorough state-of-the-art analysis of electric and hybrid vehicle powertrains: Topologies and integrated energy management strategies," *Renew. Sustain. Energy Rev.*, vol. 119, Mar. 2020, Art. no. 109596.

[11] X. Wang, L. Li, and C. Yang, "Hierarchical control of dry clutch for engine-start process in a parallel hybrid electric vehicle," *IEEE Trans. Transport. Electrific.*, vol. 2, no. 2, pp. 231–243, Jun. 2016.

[12] W. Mo, J. Wu, P. D. Walker, and N. Zhang, "Shift characteristics of a bilateral Harpoon-shift synchronizer for electric vehicles equipped with clutchless AMTs," *Mech. Syst. Signal Process.*, vol. 148, Feb. 2021, Art. no. 107166.

[13] C.-Y. Tseng and C.-H. Yu, "Advanced shifting control of synchronizer mechanisms for clutchless automatic manual transmission in an electric vehicle," *Mech. Mach. Theory*, vol. 84, pp. 37–56, Feb. 2015.

[14] C.-H. Yu and C.-Y. Tseng, "Research on gear-change control technology for the clutchless automatic–manual transmission of an electric vehicle," *Proc. Inst. Mech. Eng., D, J. Automobile Eng.*, vol. 227, no. 10, pp. 1446–1458, Oct. 2013.

[15] H. Fu, G. Tian, Y. Chen, and Q. Chen, "A novel control scheme of propulsion motor for integrated powertrain of electric bus," in *Proc. IEEE Vehicle Power Propuls. Conf.*, Sep. 2009, pp. 1496–1501.

[16] H. Fu, G. Tian, Y. Chen, and Q. Chen, "Sliding mode-based DTC-SVM control of permanent magnet synchronous motors for plug-in hybrid electric vehicles," in *Proc. IEEE Vehicle Power Propuls. Conf.*, Sep. 2009, pp. 500–505.
[17] X. Zhu, H. Zhang, J. Xi, J. Wang, and Z. Fang, "Optimal speed synchronization control for clutchless AMT systems in electric vehicles with preview actions," in *Proc. Amer. Control Conf.*, Jun. 2014, pp. 4611–4615.
[18] Z. Zhong, G. Kong, Z. Yu, X. Xin, and X. Chen, "Shifting control of an automated mechanical transmission without using the clutch," *Int. J. Automot. Technol.*, vol. 13, no. 3, pp. 487–496, 2012.
[19] J. Liang, H. Yang, J. Wu, N. Zhang, and P. D. Walker, "Shifting and power sharing control of a novel dual input clutchless transmission for electric vehicles," *Mech. Syst. Signal Process.*, vol. 104, pp. 725–743, May 2018.
[20] J. Liang, H. Yang, J. Wu, N. Zhang, and P. D. Walker, "Power-on shifting in dual input clutchless power-shifting transmission for electric vehicles," *Mech. Mach. Theory*, vol. 121, pp. 487–501, Mar. 2018.
[21] G. Li and D. Görges, "Optimal control of the gear shifting process for shift smoothness in dual-clutch transmissions," *Mech. Syst. Signal Process.*, vol. 103, pp. 23–38, Mar. 2018.
[22] C. T. Nguyen, P. D. Walker, and N. Zhang, "Shifting strategy and energy management of a two-motor drive powertrain for extended-range electric buses," *Mechanism Mach. Theory*, vol. 153, Nov. 2020, Art. no. 103966.
[23] Y. Tian, N. Zhang, S. Zhou, and P. D. Walker, "Model and gear shifting control of a novel two-speed transmission for battery electric vehicles," *Mechanism Mach. Theory*, vol. 152, Oct. 2020, Art. no. 103902.
[24] P. Teufelberger, M. Yolga, M. Ringdorfer, and E. Korsunsky, "Optimised control of a dedicated hybrid transmission," *MTZ Worldwide*, vol. 77, no. 9, pp. 36–41, Sep. 2016.
[25] Z. Zhao, P. Zhou, J. Li, Q. Huang, and K. Liang, "Upshift optimization control of dedicated hybrid transmission with P2 configuration," *Vehicle Syst. Dyn.*, vol. 1, pp. 1–24, Dec. 2020.
[26] J. Tao, Z. Huang, and J. Di, "Dual-motor hybrid dedicated transmission based on P1/P3 architecture," in *Proc. SAECCE*, 2020, pp. 1651–1669.
[27] P. D. Walker and N. Zhang, "Active damping of transient vibration in dual clutch transmission equipped powertrains: A comparison of conventional and hybrid electric vehicles," *Mechanism Mach. Theory*, vol. 77, pp. 1–12, Jul. 2014.
[28] P. Templin and B. Egardt, "An LQR torque compensator for driveline oscillation damping," in *Proc. IEEE Int. Conf. Control Appl.*, Jul. 2009, pp. 352–356.
[29] J. Fredriksson, "Improved driveability of a hybrid electric vehicle using powertrain control," *Int. J. Alternative Propuls.*, vol. 1, no. 1, pp. 97–111, Jan. 2006.
[30] F. U. Syed, M. L. Kuang, and H. Ying, "Active damping wheel-torque control system to reduce driveline oscillations in a power-split hybrid electric vehicle," *IEEE Trans. Veh. Technol.*, vol. 58, no. 9, pp. 4769–4785, Nov. 2009.
[31] X. Tian, R. He, X. Sun, Y. Cai, and Y. Xu, "An ANFIS-based ECMS for energy optimization of parallel hybrid electric bus," *IEEE Trans. Veh. Technol.*, vol. 69, no. 2, pp. 1473–1483, Feb. 2020.
[32] N. Guo, X. Zhang, Y. Zou, L. Guo, and G. Du, "Real-time predictive energy management of plug-in hybrid electric vehicles for coordination of fuel economy and battery degradation," *Energy*, vol. 214, Jan. 2021, Art. no. 119070.
[33] G. Xia, J. Chen, X. Tang, L. Zhao, and B. Sun, "Shift quality optimization control of power shift transmission based on particle swarm optimization–genetic algorithm," *Proc. Inst. Mech. Eng., D, J. Automobile Eng.*, vol. 236, no. 5, pp. 872–892, Jul. 2021.
[34] T. Ouyang, Y. Lu, S. Li, R. Yang, P. Xu, and N. Chen, "An improved smooth shift strategy for clutch mechanism of heavy tractor semi-trailer automatic transmission," *Control Eng. Pract.*, vol. 121, Apr. 2022, Art. no. 105040.
[35] G. Wang, Y. Song, J. Wang, W. Chen, Y. Cao, and J. Wang, "Study on the shifting quality of the CVT tractor under hydraulic system failure," *Appl. Sci.*, vol. 10, no. 2, p. 681, Jan. 2020.
[36] C. W. Shin, J. Choi, S. W. Cha, and W. Lim, "An objective method of driveability evaluation using a simulation model for hybrid electric vehicles," *Int. J. Precis. Eng. Manuf.*, vol. 15, no. 2, pp. 219–226, Feb. 2014.
[37] W.-H. Chen, D. J. Ballance, and P. J. Gawthrop, "Optimal control of nonlinear systems: A predictive control approach," *Automatica*, vol. 39, no. 4, pp. 633–641, Apr. 2003.

WEI REN received the B.S. and M.S. degrees in marine engineering from the Wuhan University of Technology, Wuhan, China, in 2010 and 2013, respectively. He is currently pursuing the Ph.D. degree in mechanical engineering with Nanchang University, Nanchang, China.

His research interests include the design of energy management strategy for hybrid electric vehicles and the control of the vehicle powertrain.

JUHUA HUANG received the B.S. degree in mechanical engineering, the M.S. degree in metal processing engineering, and the Ph.D. degree in material processing engineering from the Jiangxi University of Technology, Nanchang, China, in 1984, 1993, and 1998, respectively.

From 2000 to 2001, she worked as a Postdoctoral Researcher at the State Key Laboratory of Mould Technology, Huazhong University of Science and Technology. Since 1984, she has presided over, participated in and completed 13 provincial and ministerial scientific research projects. She has published more than 40 academic papers in authoritative academic journals and academic conferences, and participated in the editing of two books. Her research interests include automotive electronics, new energy vehicles, and medical equipment.

HUIHUI XU received the B.S. degree in agricultural mechanization and automation and the M.S. degree in agricultural mechanization engineering from Jiangxi Agricultural University, in 2006 and 2009, respectively.

His research interests include shiftability/drivability development and evaluation for vehicle.

JINJU YIN received the B.S. degree in mechanical engineering from Jiangxi Agricultural University, in 2009, and the M.S. degree in mechatronics engineering from East China Jiaotong University, in 2012.

Her research interests include dynamic simulation and finite element simulation.

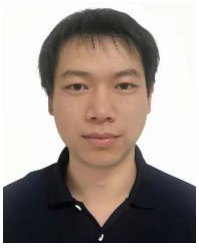

CHONG LIU received the B.S. degree in mechanical engineering from Nanchang University, in 2010.

His research interests include vehicle powertrain design and performance analysis.

LEI ZHANG received the B.S. degree in mechanical design, manufacture, and automation from the Henan University of Technology, in 2005, and the M.S. degree in materials processing engineering from Nanchang University, in 2008.

His research interest includes transmission system simulation.